5 Chapter V: Dynamic non-canonical splicing responses to neuronal depolarization stimuli

Collaboration note

Most of the work described in this chapter is currently part of the same manuscript as results in Chapter IV (Georgakopoulos-Soares et al.), which is currently under revision in Nature Communications. Ilias Georgakopoulos-Soares and I had equal contributions to these results; while Ilias Georgakopoulos-Soares quantified non-B DNA motifs across the genome, I processed publicly available RNA-seq data and splice sites. We also collaborated with Hei Yuen Wong from Hong Kong University who performed the validation experiments under the supervision of Chun Kit Kwok. Ilias Georgakopoulos-Soares and I both contributed to the experimental design. I carried out the analyses to generate all the figures presented in this chapter except the ones related to the experimental validation.

5.1 Introduction

Splicing patterns undergo dramatic changes during neuronal development, not only involving conventional splicing events, but also non-canonical splicing events such as microexons. However, neuronal alternative splicing changes are not restricted to development; mature neurons also exhibit dynamic alternative splicing changes in response to neuronal activity.

The effect of neuronal activity over gene expression and alternative splicing is often studied through the induction of neuronal depolarization by introducing high extracellular potassium ion concentrations. These potassium-induced depolarization events trigger the opening of voltage-dependent calcium channels that ultimately increase the intracellular calcium concentration. Different alternative splicing events have been associated with calcium influx triggered by depolarization, among which

several are present in genes that encode for ion channels, which have the potential to modulate neuronal electrochemical properties and function (Hermey et al., 2017; Sharma and Lou, 2011). For example, increase of intracellular calcium induces the skipping of exons 5 and 21 of NMDA receptor type 1 (*NMDAR1*) (An and Grabowski, 2007; Han et al., 2005; Lee et al., 2007) and the skipping of the so-called STREX exon present at the *KCNMA1* gene, which encodes for BK (Big Potassium) channel (Xie and Black, 2001). While NMDA exon 5 and STREX exon regulate some of the ion channel electrochemical properties (Rumbaugh et al., 2000; Traynelis et al., 1995, 1998; Vance et al., 2012), NMDA exon 21 encodes for a C-terminal protein domain (C1) that promotes *NMDAR1* retention at the endoplasmic reticulum, preventing it reaching the extracellular membrane (Ehlers et al., 1995; Scott et al., 2001; Standley et al., 2000).

Intracellular calcium increase is a pivotal signalling process that triggers several different cellular responses, many of which are promoted by the activation of calmodulin-dependent protein kinases (CaMKs). Depolarization experiments on excitable pituitary cell line GH3 have shown that skipping of the STREX exon involves the specific activation of CaMK IV (Xie and Black, 2001), which was later described as a mediator of several exon skipping events through the activation of CAMK IV-responsive RNA elements (CaRRE) (Lee et al., 2007; Xie et al., 2005). CaRRE are *cis*-regulatory elements that are bound by hnRNP L, which in its phosphorylated form leads to depolarization-induced splicing regulation (An and Grabowski, 2007). Additional *cis*-regulatory elements have also been found and novel ones may remain to be discovered (Sharma and Lou, 2011).

In addition, the architectural splicing code can play a role in the definition of alternative splicing events associated with changes in ionic concentrations. In the particular case of neuronal microexons, there is already evidence that indicate their high responsiveness to depolarisation stimuli; RNA-seq experiment analyses have demonstrated widespread microexon skipping events after depolarization of primary cultured hippocampal neurons (Quesnel-Vallières et al., 2016). Thus I hypothesized that other non-canonical splicing features could be involved in dynamic alternative splicing changes induced by depolarization stimuli. In this chapter, the research aims are centred on the third research aim of this thesis (see section 1.7). However, since

the involvement of G4 formation in depolarization-induced alternative splicing would represent a complete novelty in the field, further analyses and experimental validations were performed to investigate associations of G4 with this alternative splicing pathway.

5.2 Results

5.2.1 Dynamic splicing responses to neuronal depolarization are associated with non-canonical features

Since non-canonical splicing events, such as microexons and circRNAs, are often differentially included in neurons, we wanted to explore how they are associated with dynamic alternative splicing responses to neuronal activity. To this end, we analysed RNA-seq experiments performed on human and mouse stem cell-derived cortical neurons (Hum-ESC^{CORT} and Mus-ESC^{CORT}), mouse developing primary cortical neurons (DIV4 Mus-PRIM^{CORT} and DIV10 Mus-PRIM^{CORT}) and aneuploid Tc1 mouse neurons (DIV10 Mus-Tc1-PRIM^{CORT}) after four hours of depolarization induced by 170mM of KCl and an L-type Ca2+ channel agonist FPL64176 (KCl/FPL) (Qiu et al., 2016). The depolarization induced by KCl/FPL treatment has been reported to lead to a strong and uniform increase in intracellular calcium concentration (>10-fold increase), which is likely to have a significant effect on the CaMK IV splicing pathway (Gaspard et al., 2008; Lee et al., 2007; Xie and Black, 2001).

5.2.1.1 Depolarization triggers genome-wide cassette exon exclusion events that are highly enriched in microexons

We used MicroExonator coupled to Whippet (Sterne-Weiler et al., 2018) to perform an integrative quantitative assessment of alternative splicing for both long exons and microexons. Splicing node quantification analyses were performed by Whippet leading to the identification of a total of 22,344 alternative splicing events, 2,633 of which corresponded to core exon differential inclusion events. Among all splicing node types from Whippet's contiguous splice graph (CSG) model, the quantification

of core exons splice (CE) nodes inclusion is a direct proxy to assess the differential inclusion of cassette exons. Further analysis of CE splicing nodes showed a bias towards cassette exon exclusion after the KCl-induced depolarization stimuli as 2,346 (89.1%) of the differentially spliced CE nodes correspond to exon exclusion events. These results are consistent with previous studies which have demonstrated exon skipping following depolarisation in individual examples (An and Grabowski, 2007; Fiszbein and Kornblihtt, 2017; Lee et al., 2007; Liu et al., 2012; Schor et al., 2009; Xie and Black, 2001), but to the best of my knowledge this provides the first genome-wide analysis demonstrating widespread exon skipping (Fig 5.1a). Interestingly, the alternative cassette exons events that were found to be triggered in response to the KCl treatment are highly enriched in microexons (Fig 5.1b), suggesting their active involvement in dynamic splicing changes in neurons.

5.2.1.2 Dynamic splicing responses to neuronal depolarization are associated with G4s proximal to splice sites

Additionally, Hum-ESC^{CORT} RNA-seq analysis showed a consistent association of G4s to depolarization-induced splicing events. We found an enrichment for differential CE splicing node inclusion[8] events when intronic G4 motifs are found within a 100 nt window from splice sites (Fig 5.1c, chi-squared test with multiple testing correction, p-value<0.001, odds-ratio=1.57). To provide further support for the findings obtained using the consensus G4 motif, we examined the distribution of G4-seq derived peaks in PDS and K^+ conditions around splice sites of differentially and non-differentially included exons. As expected, we found a consistent enrichment at the differentially included CE splice nodes (Fig 5.1 c-e). These observations are consistent with replicated analyses performed across the depolarization RNA-seq experiments from mouse cortical neuron samples (Fig 5.2). Moreover, the effect size was larger for the G4 motifs and the G4-seq derived G4 sites in the non-template strand at the 5′ss in comparison to those found at the template strand (chi-square test multiple testing correction, p-value<0.001 when using the consensus G4 motif and for both PDS and K^+ G4-seq conditions in human

[8] Herein I use the expression “differential inclusion” to refer to both inclusion and exclusion events, regardless of the bias found towards inclusion or exclusion.

neurons). Taken together, our results suggest that the presence of a G4 near the splice junction of cassette exons is associated with dynamic changes of alternative splicing in response to KCl induced depolarisation, however additional experiments will be required to prove causal effects beyond the correlations reported here.

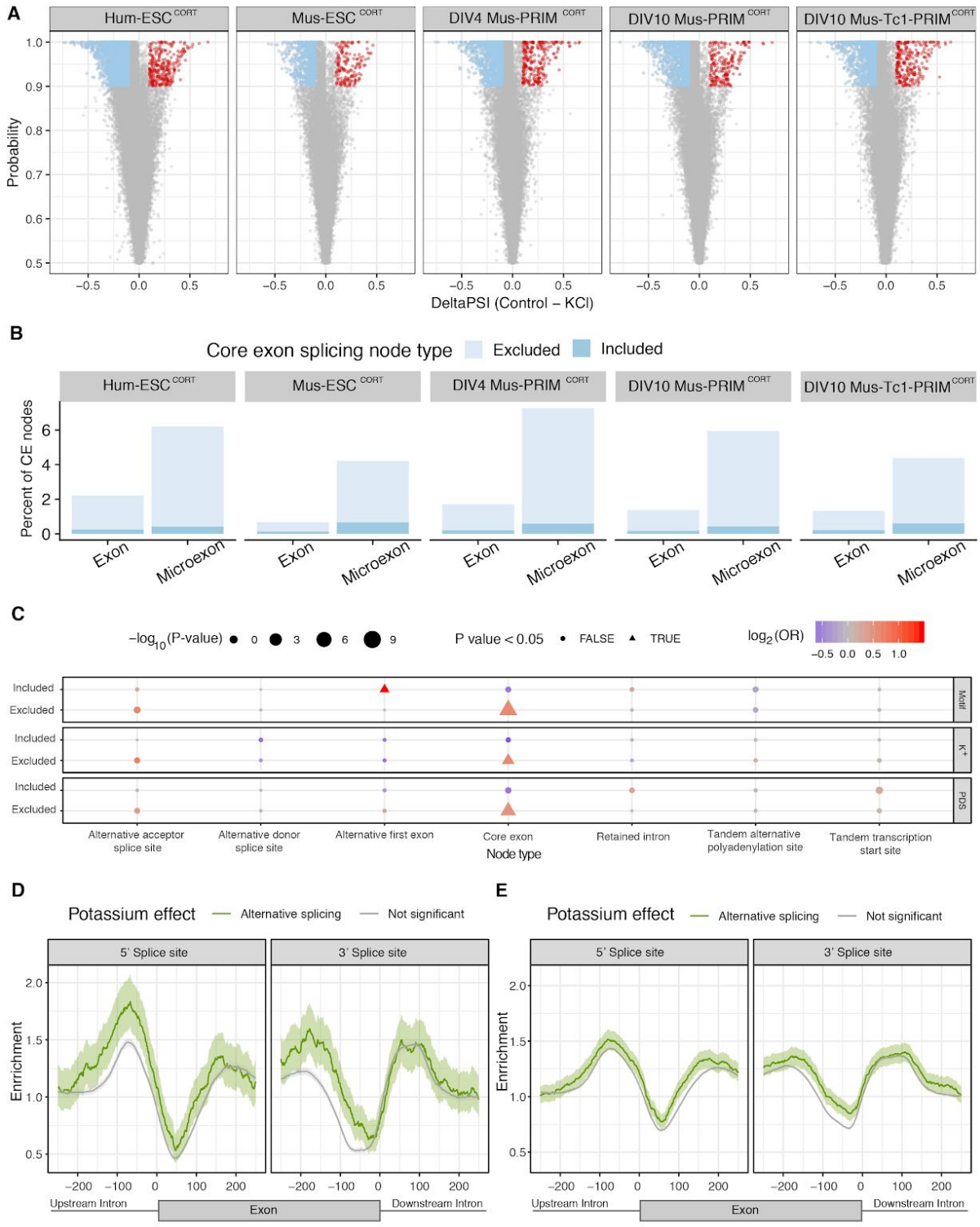

Figure 5.1: Depolarization induces genome wide exon skipping of cassette exons. Analysis of depolarization experiments across human and mouse stem cell-derived cortical neurons (Hum-ESC^{CORT} and Mus-ESC^{CORT}), mouse developing primary cortical neurons (DIV4 Mus-PRIM^{CORT} and DIV10 Mus-PRIM^{CORT}) and aneuploid Tc1 mouse neurons (DIV10 Mus-Tc1-PRIM^{CORT}) (Qiu et al., 2016). **A.** Volcano plot highlighting differentially excluded (blue dots) and included cassette

exons (red dots) after neuronal depolarization stimuli. These cassette exon inclusion quantification derives from core exon splice node quantification performed by Whippet. **B.** Differential cassette exon inclusion events after neuronal depolarization are enriched in microexons. Barplot shows the percentage of all core exons (CE) splicing nodes that correspond to cassette exon or microexon differential inclusion. Across all human and murine cortical neurons, alternative splicing changes after depolarization stimuli is significantly enriched in microexons (chi-squared tests using Yates' correction and also adjusting for multiple testing with Bonferroni multiple testing corrections, p-value < 1e-15). **C.** Differentially included splice nodes enrichment of G4 motifs in human stem cell-derived cortical neurons. Odds ratio representing the relationship between presence of G4s and alternative splicing changes. The odds-ratio significance was assessed by chi-squared tests. All p-values were calculated with chi-squared tests using Yates' correction and also adjusting for multiple testing with Bonferroni corrections. **D-E.** Enrichment of G4-seq peaks at 3' / 5' splice site vicinity for CE splicing nodes that were or were not detected by Whippet as differentially included after potassium stimulation of Hum-ESC^{CORT} (alternative spliced / not significant). G4 maps were generated after treatment with PDS (D) or KCL (E), showing consistent results. . Splice sites with G4 peaks within 100 nt were more likely to be differentially spliced following KCl treatment (chi-squared test, p-value<0.001 both at 5'ss and 3'ss). . The error bands represent 95% confidence intervals based on a binomial model.

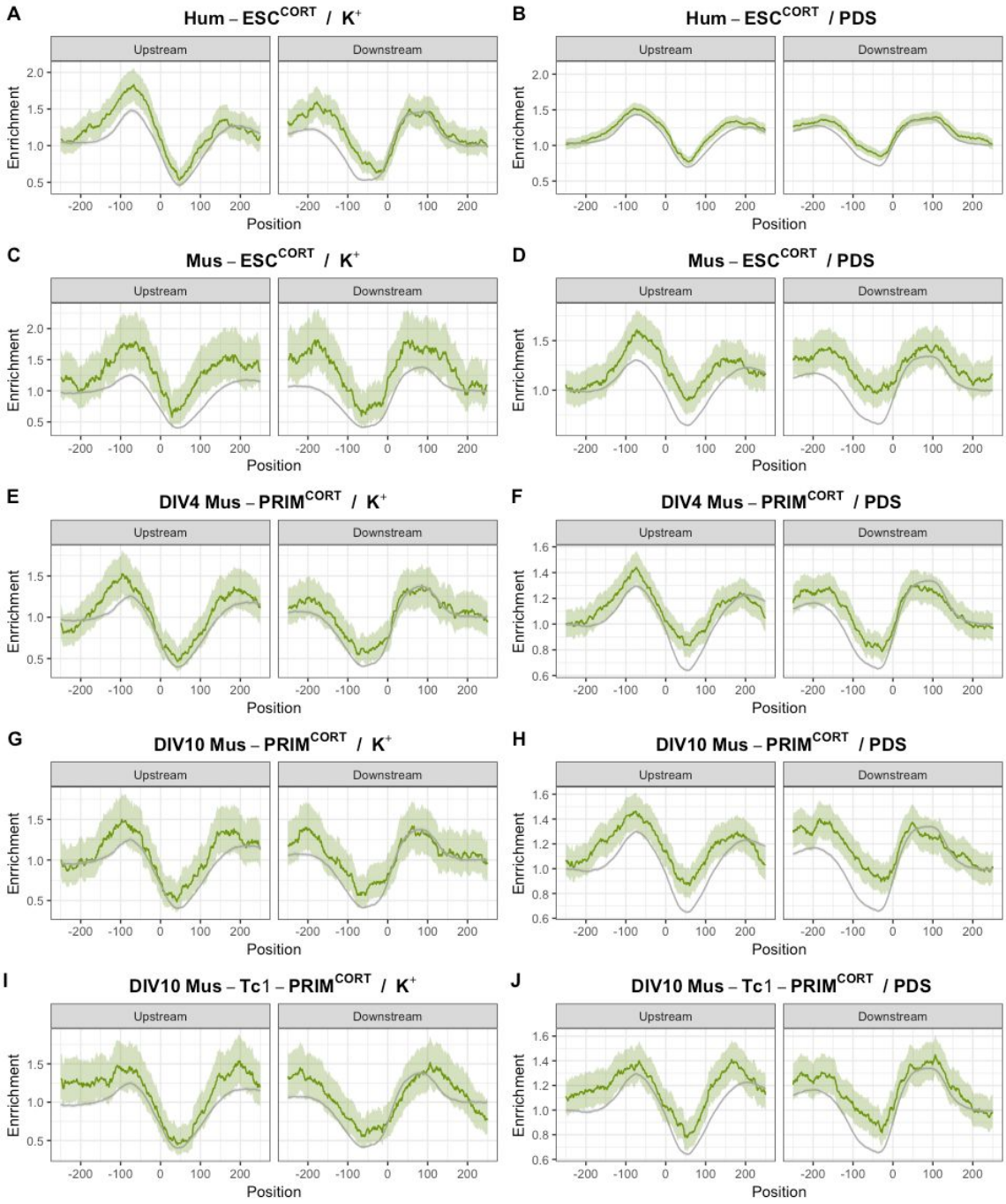

Figure 5.2: Mouse cortical neuronal depolarization experiments show G4-associated alternative splicing patterns consistent with human results. Peaks derived from G4-seq experiments under K+ and PDS are consistently enriched at the vicinity of splice sites from exons that are alternatively included after KCl-induced depolarization stimuli. The different panels correspond to different K+ and PSD G4-seq mouse experiments across different mouse cortical neurons; **A-B** Hum-ESC^{CORT} **A-B** Mus-ESC^{CORT}. **C-D** DIV4 Mus-PRIM^{CORT} **E-F** DIV10 Mus-PRIM^{CORT} **G-H** DIV10 Mus-Tc1-PRIM^{CORT}. The error bands in D-E represent 95% confidence intervals based on a binomial model.

5.2.2 Case study of G4 associated with depolarization induced exon skipping events that are evolutionarily conserved

To gain additional insights into the association between G4s and neuronal alternative splicing, we focused our attention on 3 out of 54 cassette exons that are flanked by one or more G4s and differentially included after cortical neuron depolarization in human and mouse. These exons are found at the *SLC6A17*, *UNC13A* and *NAV2* loci, and they are all flanked by one or more G4s (Fig 5.3). The criteria to select these candidates were based on the alternative splicing analysis results that we obtained from the deliparization experiments, where all three exons were differentially included in human and three or more mouse conditions. Moreover, particular focus was given to these exons since the corresponding genes have been shown to be relevant for neuronal function, which I further discuss below.

5.2.2.1 Candidate selection

SLC6A17 (NTT4/XT1) is a member of the SLC family of transporters which are involved in Na^+-dependent uptake of the majority of neurotransmitters at presynaptic neurons (Zaia and Reimer, 2009). *SLC6A17* is involved in the transport of neutral amino acids and mutations in this gene have been associated with autosomal-recessive intellectual disability (Zaia and Reimer, 2009), (Iqbal et al., 2015). Exon seven of *SLC6A17*, which is skipped after KCl treatment (Delta PSI=-0.177), has a G4 50 nt downstream of the 5′ss on the non-template strand. As the domains of *SLC6A17* include an intracellular loop, two transmembrane regions and part of extracellular domains, the KCl-induced alternative skipping of this exon may lead to functional structural changes (Fig 5.3, 5.4). Similarly, *UNC13A* encodes another presynaptic protein involved in glutamatergic transmission, and it has been associated with amyotrophic lateral sclerosis (Placek et al., 2019). We identify a G4 downstream of exon 38, which results in dramatic exon skipping (Delta PSI=-0.369), (Fig 5.3, 5.5). Finally, the third target was a G4 located downstream of exon 16 in *NAV2* (navigator protein 2), which is required for retinoic acid induced neurite outgrowth in human neuroblastoma cells (Merrill et al., 2002). Again, KCl treatment

resulted in exon skipping (Delta PSI=-0.271), which affects a *NAV2* serine rich sequence region (Fig 5.3, 5.6).

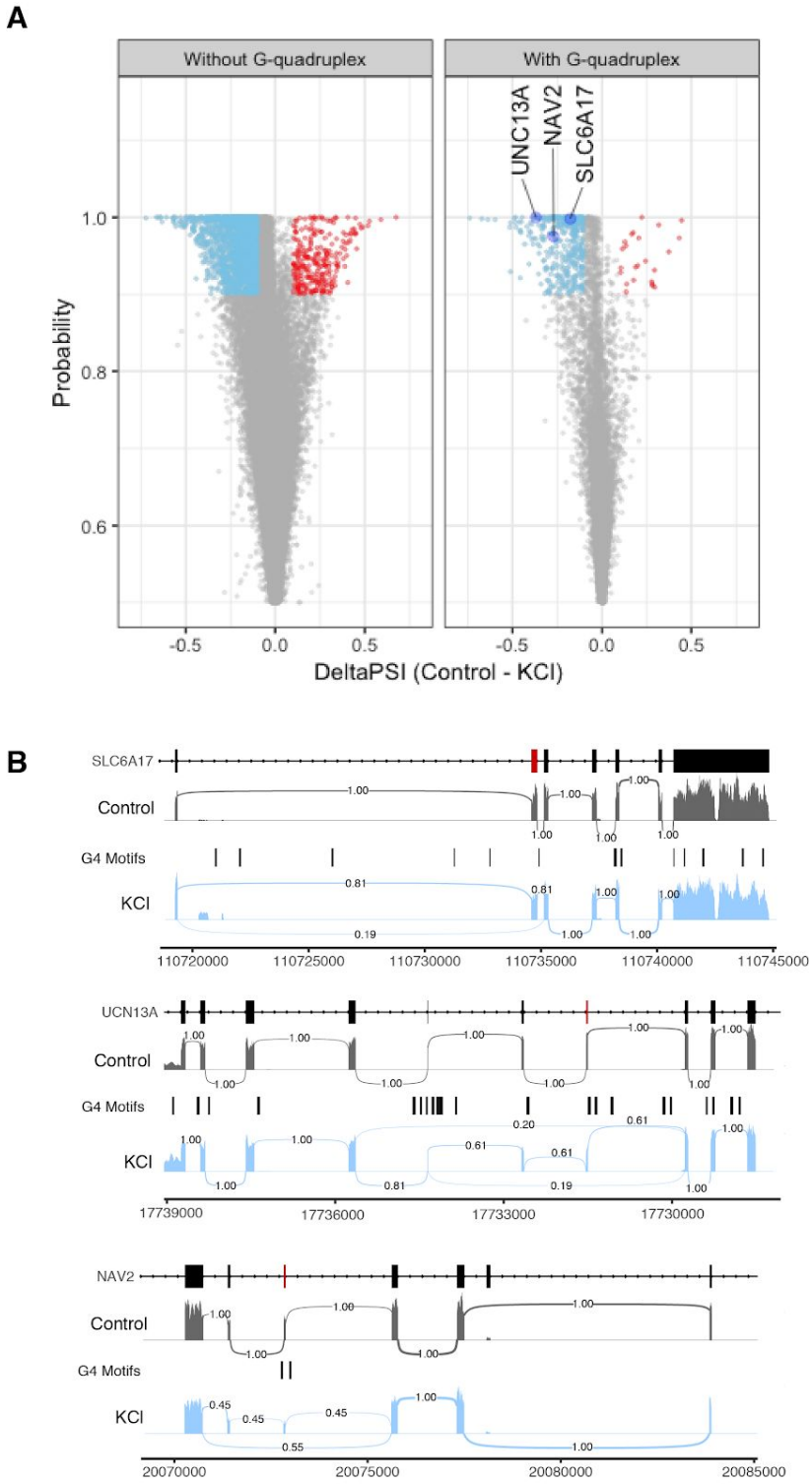

Figure 5.3: Cassette exons exhibit a strong exon exclusion pattern after KCl-induced depolarization A. Volcano plot showing differential inclusion events in presence and absence of flanking G4s and the associated probability following potassium stimulation with widespread exon skipping after depolarisation in human

neuronal cells. **B.** Sashimi plots showing alternative exon inclusion for the three candidates, namely *SLC6A17*, *UNC13A* and *NAV2* following KCl treatment. Exons flanked by a G4 that were used for validation experiments are marked in red. The numbers connecting exons represent the fraction of reads supporting each path.

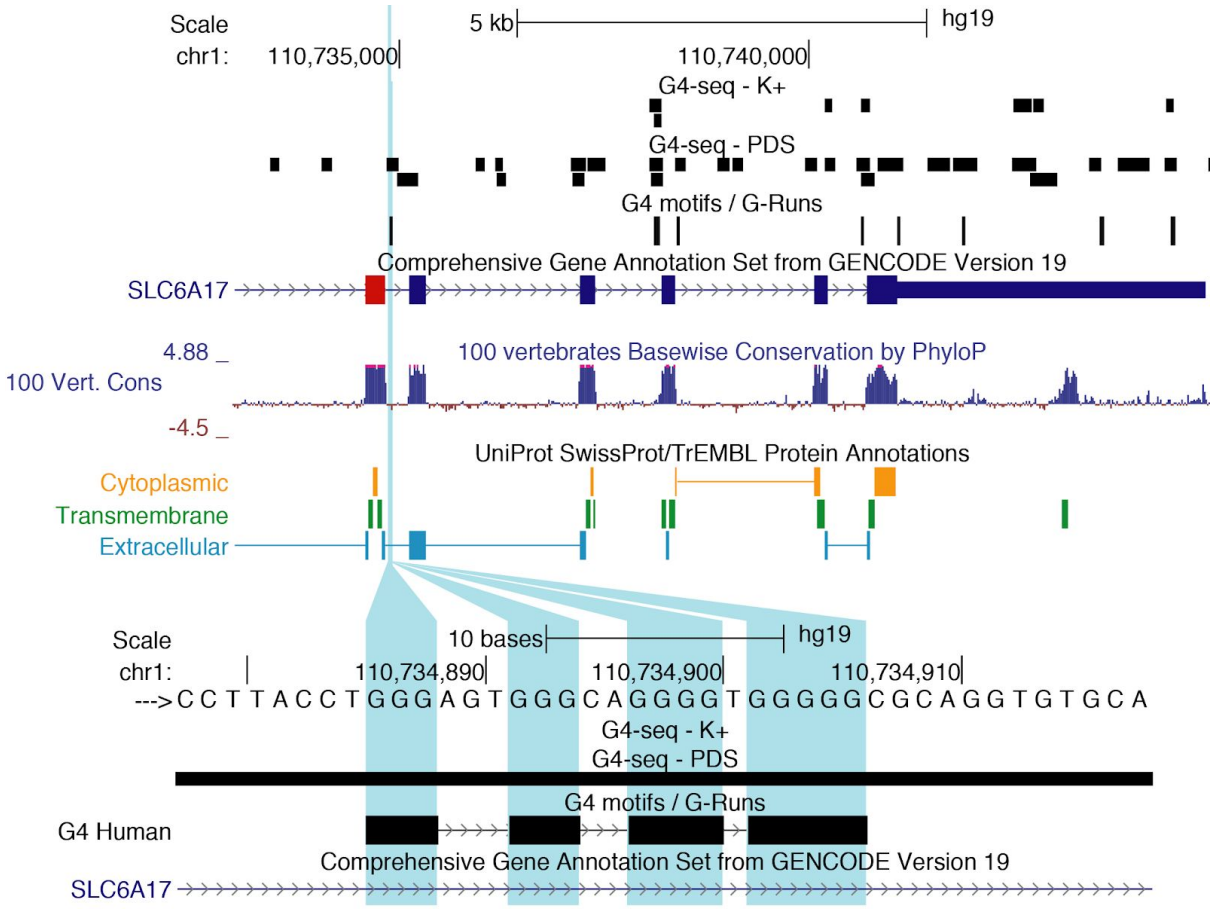

Figure 5.4: Non-template G-quadruplex motif downstream from an alternatively included SLC6A17 exon. Exon highlighted in red is skipped after KCl-induced depolarization. Downstream non-template G-quadruplex motif is highlighted in blue. G4-seq and additional UCSC tracks are shown.

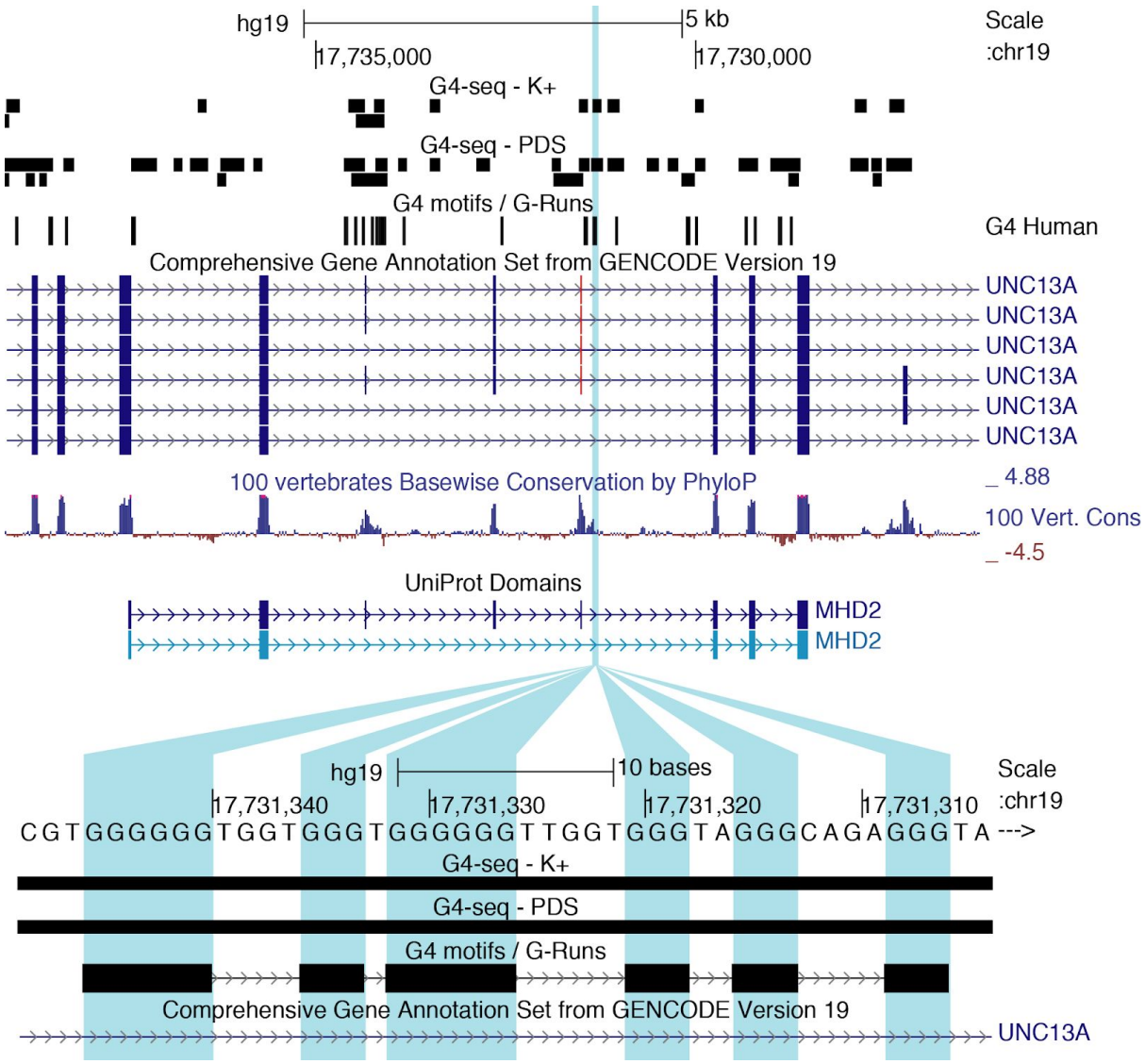

Figure 5.5: Non-template G-quadruplex motif downstream from an alternatively included *UNC13A* microexon. Microexon highlighted in red is skipped after KCl-induced depolarization. Downstream non-template G-quadruplex motif is highlighted in blue. G4-seq and additional UCSC tracks are shown.

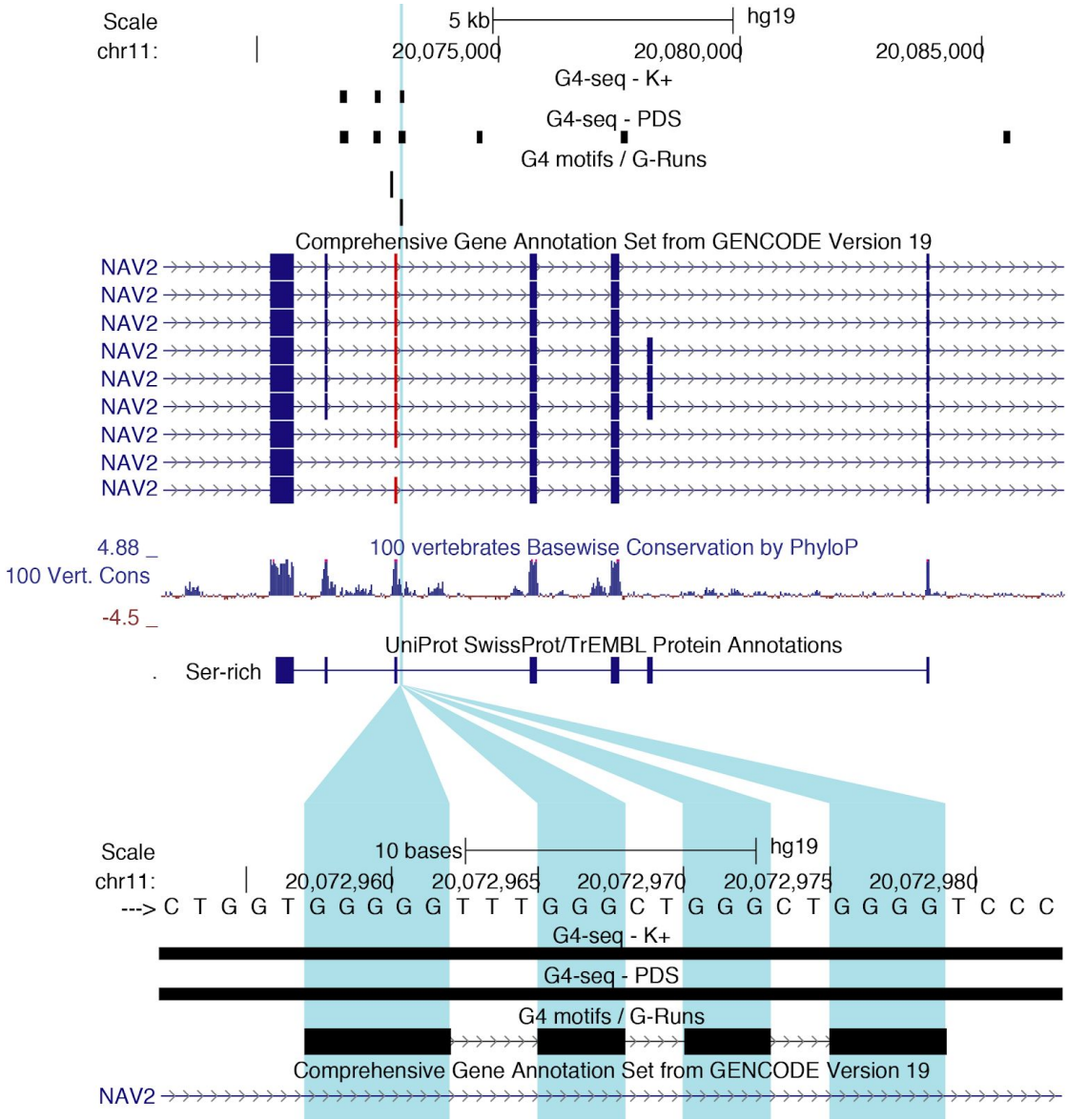

Figure 5.6: Non-template G-quadruplex motif downstream an from alternatively included *NAV2* exon. Exon highlighted in red is skipped after KCl-induced depolarization. Downstream non-template G-quadruplex motif is highlighted in blue. G4-seq and additional UCSC tracks are shown.

5.2.2.2 G4 motif sequences found at SLC6A17, UNC13A and NAV2 promote the formation of G4 structures *in vitro*

For each of the three candidates we designed RNA oligos that were used by Hei Yuen to perform multiple assays which demonstrate that these G4 not only form at the DNA level (as shown by G4-seq maps), but they are also formed at the RNA level *in vitro*. Further details the results obtained by our collaborators can be found in our preprint manuscript (Georgakopoulos-Soares et al.).

5.3 Materials and Methods.

5.3.1 Comparative analysis of RNA-seq experiment. Differential exon inclusion following depolarisation.

We analyzed available data (BioProject Accession: PRJEB19451, ENA link: ERP021488) for mouse and human ESC-derived cortical neurons, mouse primary cortical neurons from wild-type and Tc1 mice stimulated with KCl treatment and untreated followed by RNA-seq four hours post-treatment (Qiu et al., 2016). We used MicroExonator coupled to Whippet (Sterne-Weiler et al., 2018) to discover microexons and integrate them in alternative splicing analysis performed by Whippet to assess the differential inclusion of splicing nodes after KCl/FPL treatment and controls. We used absolute value of DeltaPSI greater than 0.1 and probability greater than 0.9 to define a splicing node as differentially included between treatment and controls.

We calculated the distance between the middle point of G4 motifs or G4-seq peaks from each splicing node to determine their association with G4s. Splicing nodes whose splice sites were within 100 bps of a G4 motif or 45 bps to a G4-seq peak were classified as G4 associated splicing nodes. Next, we assessed the influence of G4s to splicing changes following KCl depolarisation of human and mouse neurons by calculating the odds ratio score of each splicing node type. To determine the statistical significance of the effect we performed a chi-squared test using Yates` correction and also adjusting for multiple testing with Bonferroni corrections. The distribution of G4 motifs and G4-seq peaks was profiled around differentially included and non-differentially included core exon splicing nodes (CE). The confidence intervals were calculated using “binconf” command from “Hmisc” package in R with default parameters. Sashimi plots were generated using “ggsashimi” package (Garrido-Martín et al. 2018). Inclusion and exclusion path ratios were calculated using the total amount of spliced reads supporting each splice junction, where

inclusion paths were calculated using the average read count for splice junctions flanking each exon side.

Three putative non-template G4s found in proximity to splicing junctions and which were differentially included following depolarisation in human ESC-derived neurons and in at least one condition in mice were selected for validation experiments. These were: i) a G4 downstream of exon 7 for *SLC6A17* (chr1: 110734886-110734906), ii) a G4 downstream of exon 38 in *Unc13a* (chr19:17731307-17731346) and iii) a G4 upstream of exon 16 in *Nav2* (chr11:20072958-20072979) for which RNA oligonucleotides at the G4 locations were ordered.

The RNA oligonucleotides used were (G-runs marked in bold):

1. *SLC6A17* oligonucleotide:

GGGAGT**GGG**CA**GGGG**T**GGGGG**

2. *UNC13A* oligonucleotide:

GGGGGGTGGT**GGG**T**GGGGGG**TTGGT**GGG**TA**GGG**CAGA**GGG**

3. *Nrxn2* oligonucleotide:

GGGGGTTT**GGG**CT**GGG**CT**GGGG**